THE ASTROPHYSICAL JOURNAL, 395:642–653, 1992 August 20

POSTCOLLAPSE HYDRODYNAMICS OF SN 1987A: TWO-DIMENSIONAL SIMULATIONS OF THE EARLY EVOLUTION

MARC HERANT
Harvard-Smithsonian Center for Astrophysics, 60 Garden Street, Cambridge, MA 02138
WILLY BENZ
Steward Observatory, University of Arizona, Tucson, AZ 85721
AND
STIRLING COLGATE
Theoretical Division, Los Alamos National Laboratory, Los Alamos, NM 87545
Received 1991 August 30; accepted 1992 February 26

ABSTRACT

We present the results of simulations in two spatial dimensions of the very early phases of the explosion of SN 1987A. Starting our calculations close to the time when the prompt shock emerges from the neutrinosphere, we simulate the first few seconds of the explosion using a two-dimensional cylindrical geometry smooth particle hydrodynamics (SPH) code. The explosion energy is obtained, as in the delayed mechanism, by tapping a small fraction of the energy carried by the neutrinos produced in the making of the neutron star. The success of the explosion is determined to be sensitive to the duration of the infall, the timing of the bounce, and the subsequent neutrino heating. Using a semianalytical model for the initial structure of the collapsed object, we present two simulations that differ by the mass that has been allowed to collapse into a neutron star prior to the bounce. In the case of a short initial infall (1.37 $M_\odot$ baryon mass proto–neutron star), the explosion fails due to excessive cooling. For a longer initial infall (1.5 $M_\odot$ baryon mass proto–neutron star), the cooling is less and the explosion is successful although relatively weak [$\sim$0.35 foe (10^{51} ergs)]. We show that in this case, a successful explosion is brought about by the presence of an entropy gradient which, combined with the gravitational pull of the neutron star, leads to extremely strong instabilities. In such models, convective currents carry the deposited energy away from the neutron star and bring in new, cold material, thus preventing excessive neutrino cooling. The flow is coherent on very large scales and does not lead to microscopic mixing. The critical importance of the global circulation, for the success of the explosion, is demonstrated by the fact that similar simulations, carried out with a one-dimensional code, fizzle dramatically. It also appears that the early mixing during the explosion could account for a number of observational features of SN 1987A, such as infrared iron line profiles with extended high-velocity wings, which have so far remained unexplained.

Subject headings: hydrodynamics — stars: individual (SN 1987A) — stars: neutron — supernovae: individual (SN 1987A)

1. INTRODUCTION

From its beginnings in the 1960s, the theory of Type II supernova (SN II) explosions has been particularly slow to converge to a generally accepted solution (see Woosley & Weaver 1986 and Bethe 1990 for reviews of early work). While there has been great progress in our understanding of the remainder of the SN II phenomenon in areas such as radiation transfer or late-time hydrodynamics, work has been hampered by the nagging problem of the explosion mechanism. Very early on, two pictures emerged to power the explosion: one in which the energy is derived from the bounce of the core after it reaches supernuclear densities (Colgate & Johnson 1960), and one in which the energy is derived from the capture of a fraction of the neutrinos generated by the transformation of potential energy into internal energy during the infall (Colgate & White 1965). These two pictures are still current, although substantially modified by improvements in our knowledge of the relevant physical conditions (nuclear equation of state, weak interactions, etc.).

The most recent work on the bounce model, also known as the prompt mechanism, shows that a successful, but weak, explosion will be obtained only for a limited range of low iron core masses (Baron & Cooperstein 1990). The core of the progenitor of SN 1987A was most likely above this mass limit. Barring major changes in our understanding of the physics involved, it appears that the prompt mechanism, while being an important component of the SN II phenomenon, is incapable of generating explosions of the observed magnitude. The neutrino heating model has also failed to provide a clear-cut answer. Following the work of Wilson (1985), it was found that trapped neutrinos slowly leaking out of the proto–neutron star can revive the stalled prompt shock and thus produce what has become known as a delayed explosion. Wilson & Mayle (1989) and Mayle & Wilson (1991) present such simulations which do yield adequate explosions; however, they have not so far been reproduced by other groups.

Due to the complex physics involved and the limited amount of computational resources available, all these calculations have been performed in one spatial dimension. We argue later in this paper that extending the calculations to higher spatial dimensions is required to capture the essence of the physical mechanism responsible for the explosion: hydro-

dynamical instabilities leading to convective motions that carry the deposited energy away from the vicinity of the neutron star and bring in new, cold material which has been overtaken by the shock. This may be the key to avoid excessive neutrino cooling which has so far been the bane of attempts to model supernova explosions.

The advent of SN 1987A has given us a unique opportunity to refine our current understanding of SN IIs by confronting theory with observations. In particular, three observations can be directly connected to the explosion process itself (Arnett et al. 1989, and references therein): the neutrino detections, the amount of ^{56}Ni synthesized ($\sim 0.075\ M_\odot$), and the explosion energy ($\sim 1.4 \times 10^{51}$ ergs or 1.4 foe). These three parameters are as many clues and constraints to the explosion mechanism. Besides these three "direct" indicators, there are also a number of late-time observations of SN 1987A (light curve, line profiles, etc.) which have to be explained by any successful model.

Herant & Benz (1991, 1992; hereafter HB91, HB92, respectively) have performed various multidimensional simulations of the postexplosion hydrodynamics of SN 1987A starting from initial conditions at 300 s provided by a one-dimensional evolution of the early phase of the explosion. They have shown that regardless of the dimensionality of the hydrodynamical calculations, and within a wide range of progenitors and explosion energies, the highest velocities attained by ^{56}Ni and its decay products, ^{56}Co and ^{56}Fe, are below or barely at 2000 km s^{-1}. On the other hand, infrared (Haas et al. 1990); Spyromilio, Meikle, & Allen 1990) and X-ray (Tueller et al. 1990) observations concur to require a maximum velocity of at least 3000 km s^{-1}. We have dubbed this discrepancy the "nickel discrepancy." Further, the hydrodynamical simulations of the late-time Rayleigh-Taylor (RT) instabilities (which are known to have occurred from measurements of the light curve of SN 1987A as well as the early detection of the high-energy γ-rays) require uncomfortably large seed perturbations (HB92). If this requirement does not have a numerical cause (this seems rather unlikely given the agreement between the various numerical techniques applied to this problem), then a physical origin must be sought. Finally, it appears from polarimetry observations (Jeffery 1991), features in the line profiles (Phillips & Heathcote 1989), and speckle imaging (Papaliolios et al. 1989), that there was a global asymmetry in the expanding envelope of SN 1987A. This is corroborated by the systematic redshifts observed at early times (few hundred days) in X-ray (Tueller et al. 1990) and in infrared (Haas et al. 1990; Spyromilio et al. 1990), instead of the expected blueshift due to the intervening opacity. This large-scale asymmetry cannot possibly have its origin in the RT instabilities as their relatively small angular size (10°–15°) corresponds to at least 200 fingers for the whole ejecta which will average out any major asymmetry (HB92).

The two- and three-dimensional simulations of HB91 and HB92 rely on initial conditions provided by evolving in one spatial dimension a progenitor model (Shigeyama & Nomoto 1990) (minus a neutron star worth of matter) from $t = 0$ s to $t = 300$ s using an initial energy deposition for the explosion in the form of a thermal bomb or a piston, without regard for realism of the actual process. Because HB91 and HB92 have tried to include all the physics which potentially affect the hydrodynamics after $t = 300$ s, we conclude that the nickel discrepancy must have its origin during the first 300 s after collapse. One might be surprised at first by the idea of trying to explain line profiles measured at several hundred days after the collapse by invoking the explosion mechanism. However, while it is expected that the blast-wave hydrodynamics of a supernova depends only weakly on the specifics of the energy deposition, the nucleosynthesis of nickel is so intimately connected to the explosion process that we propose to actually use the Ni/Co/Fe line profiles coupled with multidimensional simulations as a diagnostic of what happens in the core during these crucial first few seconds.

To reproduce the light curve of SN 1987A, one-dimensional radiation transfer calculation had to assume a significant degree of chemical mixing in the ejecta. This mixing was later successfully interpreted as the results of late-time RT instabilities. In a similar manner, HB92 performed numerical simulations in two dimensions of the RT instabilities and subsequent nickel and cobalt decays assuming an arbitrary amount of nickel premixing in their initial conditions at $t = 300$ s. They found that it is necessary to uniformly premix the nickel outward to approximately $1.5\ M_\odot$ beyond the mass cut in order to get peak velocities compatible with observations Such premixing could be possible within the context of the delayed mechanism because it involves a hot, high-entropy bubble interior to low-entropy shocked matter. We show in this paper that this situation is prone to strong convective motions under the influence of the gravitational pull of the proto–neutron star. Moreover, residual inhomogeneities due to the early instabilities might be sufficient to seed the subsequent shell interface RT instabilities. As a word of caution, we should add that these convective motions are likely to affect the structure of the flow itself, hence possibly change significantly the estimates obtained by HB92. Finally, we found that, contrary to the late-time instabilities, this early convection takes the form of a very low order mode pattern that could easily allow for an asymmetric explosion with an asymmetric premixing of nickel, thus providing a natural interpretation to the global asymmetries observed in SN 1987A.

In this paper, we present two-dimensional simulations of the delayed mechanism for two post-collapse initial conditions and compare those with one-dimensional models. Our main intension is to demonstrate the importance of large-scale convection in the early stages of supernova explosions, both for the explosion process itself, and for the subsequent observational display as seen in SN 1987A. Some of our physical assumptions are crude, others are overly conservative (from the point of view of generating an explosion), and thus the results of this paper should be considered primarily as a demonstration of principle. In § 2, we describe the algorithms which we use to model the physical conditions of the delayed mechanism. At the risk of being tedious, we have paid special attention to spelling out the assumptions we made in our modeling of each physical process. In § 3, we present the results of our simulations for a range of physical and numerical parameters. Finally, § 4 is devoted to a discussion of the results and their implications and outlines potential extensions of this work.

2. NUMERICAL METHODS AND PHYSICAL CONDITIONS

The two-dimensional simulations we present here were run with a cylindrical geometry smooth particle hydrodynamics (SPH) code identical in structure to the one used in HB91 and described in HB92. One-dimensional simulations were performed with a second-order, explicit, grid-based, Lagrangian code which is described in Benz (1991). For comparison purposes, all physical processes such as neutrino heating and cooling, equation of state, etc., are implemented in identical

ways in both the SPH and the one-dimensional codes. However, the Lagrangian code does not include any type of algorithm (mixing-length or other) to simulate convective energy transport. Thus, the primary, and probably only, significant difference between the codes is that the two-dimensional SPH scheme allows for the effect of vortex motion and hydrodynamic mixing, while the one-dimensional Lagrangian method does not. The mass resolution in the Lagrangian one-dimensonal code is of order $\delta m = 5 \times 10^{-4}$ $M_\odot$ and remains constant throughout the grid. In the SPH code, the particles are initially laid down in such a way that the masses increase linearly with the distance from the z-axis (a natural choice in two-dimensional cylindrical geometry). At early times, in the neighborhood of the proto–neutron star, the masses of the particles are of order $\delta m = 10^{-6}$ $M_\odot$, but become larger at greater radii. We have checked numerical convergence by doubling and halving the number of particles compared to our standard runs of $\sim 10^4$ particles. There were no changes in the bulk features of the flow.

Most of our calculations in two dimensions were performed in a computational space limited to a 120° wedge centered on the equatorial plane which has a volume equal to $3^{1/2}/2$ of the total volume. In some cases, we have performed experiments in a 60° wedge containing half of the total volume. We do not run simulations with the complete, 180°, computational space in order to avoid numerical artifacts introduced by the fundamentally pathological (in SPH) z-axis boundary. The boundary conditions are periodic, particles being able to cross on one side and reenter on the other. The gravitational force is always radial, and its magnitude is computed from the total mass inside the radius of each particle. This treatment should be adequate if the mass distribution remains close to spherically symmetric. In addition, at small radii, where the flow is most asymmetric, gravity is dominated by the presence of the proto–neutron star; hence, we believe this assumption to be good enough. At late times ($t > 1$ s), the expansion decreases the resolution so much that the code does not resolve the proto–neutron star anymore. At this point, we introduce a softening length for the neutron star gravity which allows us to pursue the simulation to later times since the time step is no longer set by time scales in the region close to the surface of the neutron star. Since at this time all the "action" occurs far away from the neutron star (except possibly for accretion; see § 2.5 for a discussion of this issue), this softening does not change the nature of the simulation. Finally, the prescription we use for the nucleosynthesis of ^{56}Ni is that all material which passes from a temperature above $T = 5 \times 10^9$ K to below that is assumed to "freeze" into ^{56}Ni.

2.1. *Initial Conditions*

In order to be able to model the delayed mechanism without having to simulate the core collapse phase itself and the ensuing formation of a proto–neutron star, we have resorted to a simplified procedure. We calculate our initial conditions, corresponding approximately to the time when the prompt shock emerges from the neutrinosphere using the following recipe. We start with a progenitor model supplied to us by K. Nomoto. This is the same model which was used to simulate late-time instabilities of SN 1987A in Hachisu et al. (1990), HB91, and HB92. We collapse the progenitor with a one-dimensional model in a semianalytic way; every shell of matter start to move inward at two-thirds of the free-fall velocity as soon as the rarefaction wave, originated by the collapse of the central parts and propagating outward at sound speed, reaches the corresponding radius. The factor of two-thirds comes from Yahil (1983), in which it is found analytically that the terminal velocity of infalling matter remains below the free-fall speed. Numerical simulations of the collapse (Arnett 1977; Bruenn 1985) agree with this analysis. In this simple model, it is straightforward to compute the radius $r(t)$ of a given shell:

$$\begin{cases} r(t) = r_0 & t < \tau_s(r_0)\,, \\ r(t) = r_0 + \displaystyle\int_{\tau_s}^{t} \left(\frac{dr}{dt}\right) dt & \tau_s(r_0) < t < \tau_s(r_0) + \dfrac{3}{2}\,\tau_{\rm ff}(r_0)\,, \\ r(t) < R_{\rm NS}\ \text{(in Neutron Star)} & \tau_s(r_0) + \dfrac{3}{2}\,\tau_{\rm ff}(r_0) < t\,, \end{cases}$$

with for the infall velocity:

$$\frac{dr}{dt} = -\frac{2}{3}\left[2GM\left(\frac{1}{r} - \frac{1}{r_0}\right)\right]^{1/2},$$

and the two time scales are given by

$$\text{Sound crossing time:}\quad \tau_s(r_0) = \int_0^{r_0} \frac{dr}{c_s(r)}\,;$$

$$\text{Free-fall time:}\quad \tau_{\rm ff}(r_0) = \frac{\pi}{2}\,\frac{r_0^{3/2}}{\sqrt{2GM}}\,.$$

In these expressions, M is the mass interior to a shell and $R_{\rm NS}$ is the radius of the proto–neutron star whose inner structure we do not model. Once $r(t)$ has been computed, the mass conservation equation can be used to obtain the corresponding shell density. Finally, we obtain the shell temperature (or specific internal energy) by assuming that this process is taking place adiabatically.

Admittedly, this picture is an oversimplification of the real collapse. As we show below, the results strongly depend on exactly when the bounce takes place and the neutrinos start heating the material surrounding the proto–neutron star. A consistent collapse model and corresponding spectrum of the emerging neutrinos is therefore imperative in order to determine the full solution. This work is currently in progress. The purpose of this paper being more a demonstration of principles than an actual realistic calculation, we have chosen two initial conditions that span the range of typical results: failure and success.

The two models chosen as initial conditions to our simulations, correspond to the infall solution taken at $t = 0.4$ s and $t = 0.7$ s which in turn correspond to a proto–neutron star baryon mass of 1.37 $M_\odot$ and 1.5 $M_\odot$ (Fig. 1), respectively. In the rest of this paper, these two initial conditions are referred to as model A and model B. At the start of each simulation, we assume that the bounce shock is located at the proto–neutron star surface and has temporarily stopped the accretion flow. Notice that we neglect the initial kinetic energy of the bounce shock which is not quite correct, since from the calculations of Mayle & Wilson (1988) and others, it is known that the bounce persists out to a few hundred kilometers, beyond the proto-neutron star surface. Our approximation therefore, if anything, tends to make the explosion even more difficult.

Finally, these models are mapped into two-dimensional representations suitable for the SPH code. No perturbations are introduced, since numerical noise was found largely sufficient to seed the instabilities.

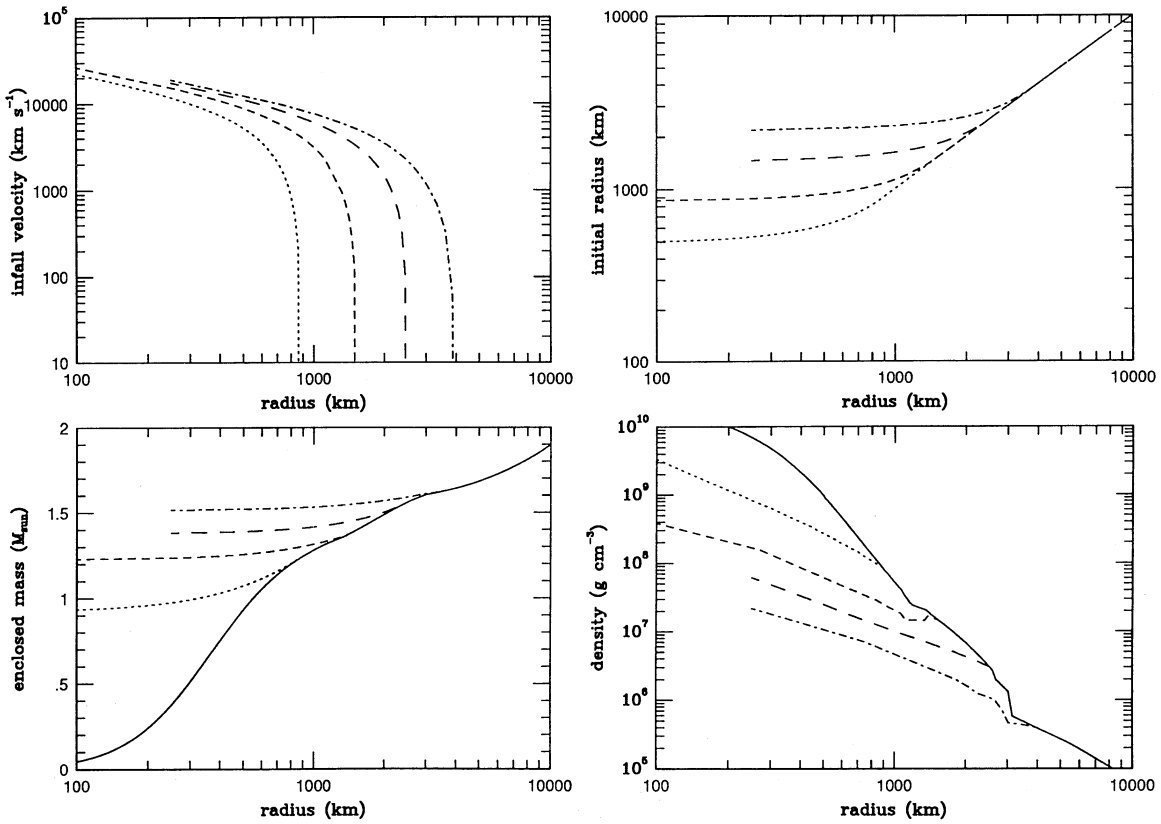

FIG. 1.—Infall solutions at $t = 0.0$ s (*solid line*), 0.1 s (*dots*), 0.2 s (*short dashes*), 0.4 s (model A, *long dashes*), and 0.7 s (model B, *dash-dot*) after the onset of collapse

2.2. *Equation of State*

The huge range of densities and temperatures encounted during the explosion requires a fairly sophisticated treatment of the equation of state. However, since we do not model the proto–neutron star interior, our equation of state does not involve a nuclear component. For temperatures below 2×10^9 K, we use an equation of state which simply includes perfect gas and radiation pressure ($P = aT^4/3 + \rho RT/\mu$). For temperatures above that, the equation of state which we use includes the effects of gas pressure, radiation pressure, electron degeneracy (including partial degeneracy), Coulomb corrections, and electron position pair creation (Fig. 2). In addition, the proper chemical composition for material at a given temperature is calculated by assuming that this material is always a mixture of neutrons, protons, α-particles, and iron in nuclear statistical equilibrium (NSE, see Fig. 3). We assumed an initial composition of 100% iron at $t = 0$. The energy needed to dissociate this iron is treated as a sink term in the energy equation:

$$\Delta U = 2.29 \times 10^{18} x_\alpha + 1.81 \times 10^{19} x_p \text{ ergs g}^{-1} ,$$

where x_α and x_p are the alpha particles and free protons mass fractions. The first term in this expression corresponds to the energy needed to dissociate iron into alpha particles and the second term to the dissociation of the iron into protons and neutrons. The assumption of a 100% initial iron composition is of course incorrect when the material from the oxygen shell becomes involved in nuclear reactions, but it nevertheless accounts for most of the energetics adequately because the difference in binding energy per nucleon between oxygen and iron is similar to that between oxygen and helium. Further, the bulk of the dissociation energy is taken up by the transition from alpha particles to free nucleons. We note again that, if anything, this assumption will also tend to make the explosion more difficult. As an ultimate check, we have run one test case where the NSE condition was used with oxygen replacing iron as the heavy nucleus. No significant changes were registered.

2.3. *Neutrino Heating*

The heating of the exterior (to the proto–neutron star) matter modeled in these calculations takes place through the

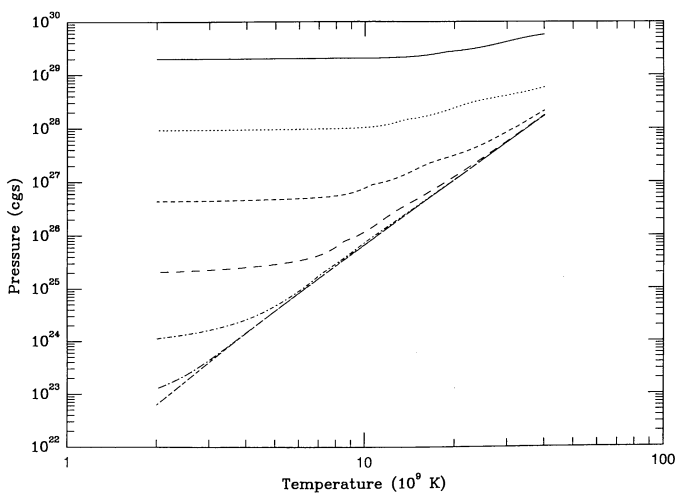

FIG. 2.—P vs. T from our equation of state including the effect of change in composition (see text for details) for densities ranging from 10^{11} to 10^5 g cm^{-3} (*top to bottom*).

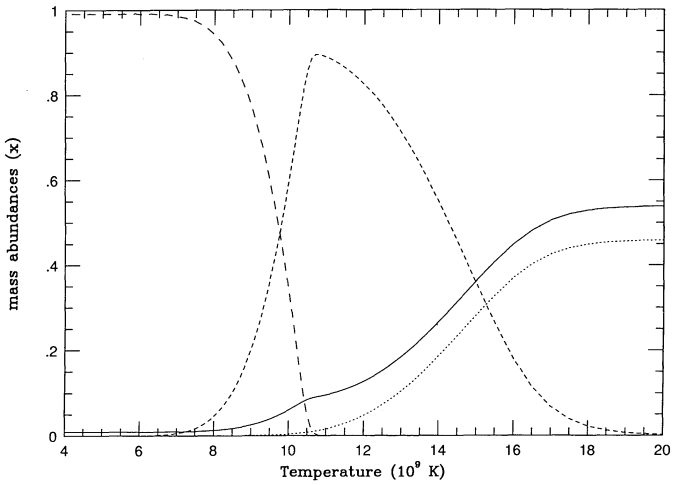

FIG. 3.—NSE abundances of iron (*long dashes*), α-particles (*short dashes*), free protons (*dots*), and free neutrons (*solid*) as a function of temperature for $\rho = 10^9$ g cm^{-3}.

absorption of a small fraction of the neutrino energy carrying outward the enormous gravitational energy released by the making of a neutron star. In our simulations, we model this as a central background neutrino point source with a luminosity and temperature time dependence given by model 54 of Burrows (1988; see also Bludman & Schinder 1988). This model corresponds to the post-collapse cooling of a proto–neutron star of 1.4 $M_\odot$ baryon mass. The luminosity and temperature are assumed equal for all neutrino species. Furthermore, because at most only 10% of the electron neutrinos emerging from the proto–neutron star deposit their energy in the exterior matter (less for other neutrino species), we do not take into account the attenuation of the neutrino flux with radius due to partial absorption. We also neglect the neutrinos generated by the cooling of this matter, so that there is no accretion-induced neutrino luminosity in our models. Note that this flux is below what is required by the neutrino bursts observations.

There are two types of processes which lead to neutrino heating: neutrino absorption by free nucleons (1, 2) and neutrino electron (or positron) scattering (3, 4) (NES):

$$\begin{cases} n + \nu_e \rightarrow p + e^- & (1) \\ p + \bar{\nu}_e \rightarrow n + e^+ & (2) \\ e^- + \nu_e \rightarrow e^- + \nu_e & (3) \\ e^+ + \nu_e \rightarrow e^+ + \nu_e & (4)\,. \end{cases}$$

Reactions 1 and 2 also occur with nucleons bound in a nucleus. However, they generally lead to the rapid reemission of a neutrino of similar energy to the one which was absorbed (Bethe 1990), thereby preventing a net gain of energy. Neutrinos can interact with nuclei through elastic scatterings. Despite the enhanced cross section due to coherent scattering, this does not add to the heating directly because the large ratio between nucleus rest mass and neutrino energy leads to an extremely low recoil energy. However, these larger cross sections can contribute to neutrino trapping and thus extend the heating by processes 1–4. We have also neglected neutral current nuclear disintegration which would add ~10% to the energy deposition according to Bruenn & Haxton (1991). We do not take into account the neutrino pair annihilation process ($\nu_e + \bar{\nu}_e \rightarrow e^- + e^+$; see Goodman, Dar, & Nussinov 1987; Mayle & Wilson 1991; Janka 1991) because it is dependent on the structure of the neutrinosphere itself which we do not model. Since we have opted for a conservative approach in this paper, we have not included any contribution from this heating mechanism.

The cross section for neutrino absorption (1, 2) is $\sigma = 9 \times 10^{-44} \epsilon_\nu^2$ cm^2, where ϵ_ν is the neutrino energy in MeV. We set $\epsilon_\nu = 3T_\nu$ with T_ν the temperature of the neutrinosphere in MeV for which we adopt the values given by Burrows's model 54. This assumption is artificial since the distribution of neutrinos emerging from the proto–neutron star is not always thermal, but this prescription has the advantage of being simple, while correctly accounting for the main features of the problem. The heating rate is then

$$\left(\frac{du}{dt}\right)_{\text{abs.}} = 4.8 \times 10^{32} \frac{L_{\nu_e}(\text{foes s}^{-1})}{4\pi r^2} T_\nu^2 (x_p + x_n) \text{ ergs s}^{-1} \text{ g}^{-1}\,.$$

The mass fraction of free nucleons $(x_p + x_n)$ is constantly updated for each smooth particle as a fraction of its temperature and density by assuming NSE.

The cross section for NES (3, 4) is $\sigma = 8 \times 10^{-44} T \epsilon_\nu$ cm^2, where T is the matter temperature and both T and ϵ_ν are in MeV. To compute the electron and positron concentrations, we use approximations for the Fermi integrals from Takahashi, El Eid, & Hillebrandt (1978) with $Y_e = 0.5$. Note that even when the materials is fairly degenerate, there will not be significant end-state blocking for the process, since scattering by a neutrino should almost always be sufficient to lift an electron above the Fermi sea. We give the following limiting expressions; if pairs dominate,

$$\left(\frac{du}{dt}\right)_{\text{NES}} = 1.1 \times 10^{40} \frac{L_{\nu_e}(\text{foes s}^{-1})}{4\pi r^2} (T_\nu - T) \frac{T^4}{\rho} \text{ ergs s}^{-1} \text{ g}^{-1}\,;$$

and if charge neutrality electrons dominate,

$$\left(\frac{du}{dt}\right)_{\text{NES}} = 1.4 \times 10^{32} (T_\nu - T) T \text{ ergs s}^{-1} \text{ g}^{-1}\,.$$

The factor $T_\nu - T$ comes from an ad hoc efficiency factor $(T_\nu - T)/T_\nu$ for the energy transfer in the scatterings. We have found in our simulations that, as far as the energy budget of the explosion is concerned, absorption heating strongly dominates NES heating (by a factor of about 5–10).

2.4. *Neutrino Cooling*

Cooling takes place through processes which create neutrinos which then escape from the star. Two cooling mechanisms are available: the capture of leptons by nucleons and photo, pair, and plasma neutrino emission processes. Cooling works against the success of the explosion in two ways; evidently, it decreases the available energy for expansion, but also, it determines the amount of accretion onto the proto–neutron star which has the effect of removing support from the explosion shock. However, it is also possible that the accretion rate partly determines how much energy is available to power the explosion (see § 2.5).

The most important cooling process, which is an order of magnitude more effective than the pair neutrino cooling, is provided by electron followed by positron capture on protons

and neutrons:

$$p + e^- \rightarrow n + \nu_e \quad (5)$$

$$n + e^- \rightarrow p + \bar{\nu}_e \quad (6)\,.$$

The cross section for both processes with the nucleon at rest is $\sigma = 4.5 \times 10^{-4}\epsilon_\nu^2$ cm^2 where ϵ_ν is the energy of the neutrino in MeV. Note that reactions 5 and 6 are just the inverse processes from reactions 1 and 2. The corresponding cross section is halved because in 5 and 6, half the states are forbidden since the neutrino can only have a left-handed helicity. In our calculations, we use the expressions given by Takahashi et al. (1978) with the assumption that $Y_e = 0.5$. This latter assumption is warranted to the extent that, (*i*) we know that large amounts of ^{56}Ni were produced during the explosion of SN 1987A, and (*ii*) since reaction 5 tends to dominate the cooling losses by absorption, if anything we overestimate the cooling by assuming Y_e larger than it should be. We give here an approximate evaluation of the capture losses assuming that $k_B T \gg m_e c^2$, and the mass difference between protons and neutrons is negligible (this is taken into account in the actual calculations, though):

$$\left(\frac{du}{dt}\right)_{\text{capture}} = -2.0 \times 10^{18} T^6 (x_p + x_n) \times \left[1 + \frac{1}{240}\left(\frac{\eta^6}{6} + \frac{5}{6}\pi^2\eta^4 + \frac{7}{6}\pi^4\eta^2\right)\right] \text{ergs s}^{-1}\text{ g}^{-1}\,,$$

where T is the matter temperature in MeV, $(x_p + x_n)$ is the free nucleon mass fraction, and $\eta = \mu/k_b T$, with μ the chemical potential updated for every particle at each time step.

Our treatment of cooling via the photo, pair, and plasma neutrino emission mechanisms is taken straight out of Schinder et al. (1987). We use their fitting formulae for 10^{10} K $< T < 10^{11}$ K with, once again, $Y_e = 0.5$; the reader is referred to their paper for the details. An estimate of the cooling losses at high temperatures is given by the following expression:

$$\left(\frac{du}{dt}\right)_{\text{ppp}} = -1.9 \times 10^{25} \frac{T^9}{\rho} \text{ ergs s}^{-1}\text{ g}^{-1}\,,$$

where T is, as before, the matter temperature in MeV. Recently, Braaten (1991) has shown that these cooling rates have been underestimated by a factor of about 3 in the ultrarelativistic regime. As a check, we have run a simulation with the rates from Schinder et al. (1987) tripled. There were no significant changes. Nevertheless, this increase in cooling at very high temperatures may be important for the detailed study of accretion onto the proto-neutron star.

2.5. *Proto–Neutron Star and Accretion*

In our simulations, the proto–neutron star surface is represented by a fictitious spherical boundary with a radius which varies linearly from 55 km to 15 km in a time of 0.5 s. To determine the pressure gradient across the boundary we assume hydrostatic equilibrium. The boundary is reflective as the sign of the radial velocity is reversed across it. Particles which reach a density greater than 6×10^{10} g cm^{-3} are assumed to represent matter which is on its way to neutron degeneracy and are removed as accreted mass. In order to check how our results are affected, we have tried a number of other boundary conditions and accretion schemes. Some simulations were run with a constant pressure accross the boundary, and with a static boundary instead of a reflective boundary (i.e., $v^r_{\text{out}} = 0$ instead of $v^r_{\text{out}} = -v^r_{\text{in}}$). In the case of the constant pressure boundary condition, we have used an accretion scheme in which particles which crossed the boundary were accreted. We have also tried cases in which accretion was modeled by a reduction on a cooling time scale of the mass of the particle in the direct vicinity of the neutron star (similar to Anzer, Borner, & Monaghan 1987; see also Herant 1992). All these approaches have yielded similar results. This seems to indicate that beyond the fact that the proto–neutron star consists of a hard wall in which matter can be incorporated only by reaching neutron degeneracy, the details of the boundary conditions do not influence much the way the delayed mechanism operates within the framework of our simulations.

There are some shortcomings in our approach to model the proto–neutron star surface and the accretion. As mentioned in § 2.3, we are not in a position to model the $\nu\bar{\nu}$ annihilation process which could make a significant contribution to the explosion energy (Mayle & Wilson 1991). In simulations which do yield explosions, the density in the "hot bubble" drops dramatically and as a result the concentration of particles near the surface decreases. In addition, the radius of the proto–neutron star is also shrinking with time. Such reduced spatial resolution at late times prevents us from properly resolving the stratification of the atmosphere around the neutron star. This may be important to the explosion process since the base of the atmosphere corresponds to the region of most intense cooling. This is due to the fact that neutrino processes are strongly dependent on energy, so that in both the case of a degeneracy—or a thermally supported atmosphere—there is either a peak in Fermi energy or in temperature (and hence in cooling) at the bottom of atmosphere surrounding the proto–neutron star. In turn, the peak cooling rate determines the accretion rate, and thus, poor resolution of this peak translates into large errors in the mass accretion rate. As explained above, although our simulations are successful in modeling the peak correctly early on ($t \leq 100$ ms), this is no longer true at later times.

In line with the conservative approach of this paper, we have considered only heating by neutrinos diffusing out of the cooling proto–neutron star (see § 2.3). It is, however, likely that neutrinos from post-collapse accretion will provide a significant (if not determining) contribution to the energy input which powers a supernova explosion. A detailed analysis and implementation of accretion physics is beyond the scope of this paper which is intended mainly as a preliminary study of the delayed mechanism in two dimensions. However, we briefly outline here a possible scenario. Accretion occurs when the pressure gradient is unable to match the gravitational forces. Thus, the inability to establish a static atmosphere depends on the energy losses. At it cools, the entropy of the base of the atmosphere decreases. Consequently, hydrostatic equilibrium is restored by adiabatic compression which attempts to maintain pressure through an increase in temperature (or if degeneracy has set in, an increase of the Fermi energy), thereby leading to increased cooling losses. This situation is clearly unstable and will give rise to an ever higher rate of infall, with emission of neutrinos of ever higher energy. The factors which limit such a runaway are the mass input rate, the "Eddington limit" due to opacity to high-energy neutrinos, and the maximum, free-fall velocity of matter. We therefore obtain an additional source of high-energy (and thus efficient for energy deposition in the ejecta) neutrinos with which to power the explosion.

These equations are explored further by Colgate, Herant, & Benz (1992) and will be addressed more thoroughly in a future paper.

3. RESULTS

As mentioned in § 2.1, we have chosen two different initial conditions for our simulations; one corresponds to 0.4 s of infall with a proto–neutron star baryon mass of 1.37 $M_\odot$ (model A), and the other corresponds to 0.7 s of infall with a proto–neutron star baryon mass of 1.5 $M_\odot$ (model B). The outcome of the evolution of each model is very different: model A fizzles while model B leads to a successful explosion. This underlines the importance of the post-collapse structure (at bounce) and the timing of the neutrino leakage. For the purpose of this paper, we will consider model A as a generic fizzler and model B as a generic exploder. We expect that these two models will exhibit the main features of each outcome. A definitive analysis, however, will require a seamless model going from the onset of collapse to the explosion, which we are in the process of working out. In this section, we describe the behavior of the two models; we analyze their features and their implications in § 4. Note also that for now on in this paper, $t = 0$ at bounce.

Our results for model A can be summarized as follows. The shock moves out to $r \sim 100$ km at $t \sim 15$ ms before stalling and then gradually retreating (Fig. 4). Although there are hints of cells forming, convection never develops significantly because cooling losses dominate early, in the entire postshock region. Neutrino heating does not get a chance to produce an inward directed entropy gradient, as required for convective instability. Receiving no energy input, the shock is starved and dies. The causes of this fizzle lie with the dependency of the electron capture cooling on high powers of $\eta = \mu/k_B T$ (if the Fermi energy is large, neutrino cooling is enhanced, § 2.4) coupled to a large inward momentum flux. The relatively early release of neutrinos comes as the infall has not thinned out very much, resulting in a very high density region between the proto–neutron star surface and the accretion shock. As this material which is already degenerate cools, degeneracy increases and the cooling rate follows. It is probable that were we to evolve Y_e in the code, proton depletion would decrease the cooling losses. However, heating requires neutrino capture by neutrons and will therefore produce protons. One is left in the unenviable position that better heating means better cooling.

As seen in Figure 5, model B follows a completely different evolution than model A since it yields a successful explosion. At a very early time after the beginning of the simulation ($t \sim 15$ ms), when the shock is at a distance from the proto–neutron star surface which is of the same order as the proto–neutron star radius, four approximately spherical convection cells have already formed. By $t \sim 35$ ms, the shock has moved out to a radius $r \sim 300$ km, and the four cells have stretched in the radial direction, but they do not extend any more to the very surface of the proto–neutron star. At small radii, the combined effects of degeneracy and high temperature increase the cooling losses so that they dominate the heating. This region is therefore not subject to convective instabilities, and slowly dumps matter onto the proto–neutron star, while the rest of the volume behind the shock continues to convect. In that sense, the mass cut is dynamically established during the delayed mechanism as the location where cooling is equal to heating. Above that radius low-entropy matter is channeled in narrow inflows and, once heated by the proto–neutron star neutrinos, the matter is ejected by buoyancy in wide outflows. Thus, heated material is continuously removed from the vicinity of the proto–neutron star and replaced by cold matter from the shocked, infalling envelope (see Fig. 6).

At later times ($t \sim 100$–500 ms, Fig. 7), convective cells merge so that there remain a single inflow and a single outflow. The inflow consists of a rarefaction wave moving out behind

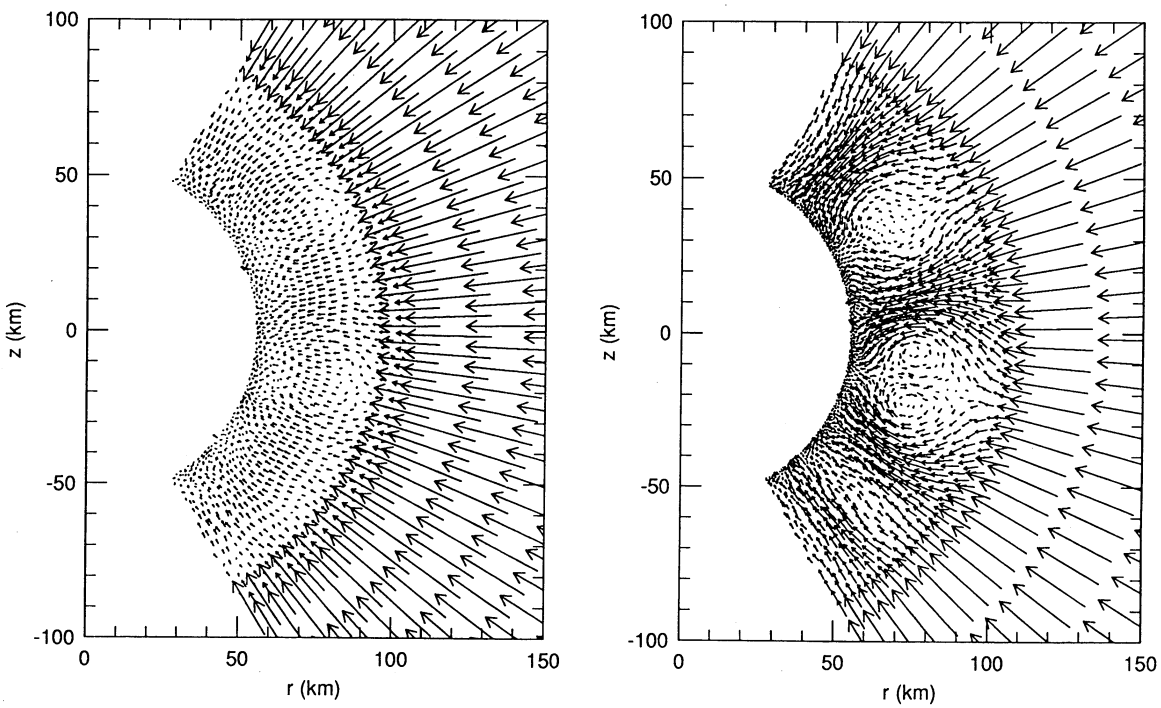

FIG. 4.—Velocity plots for model A at $t = 11$ ms (*left*) and $t = 20$ ms (*right*). Velocities are scaled independently for each plot.

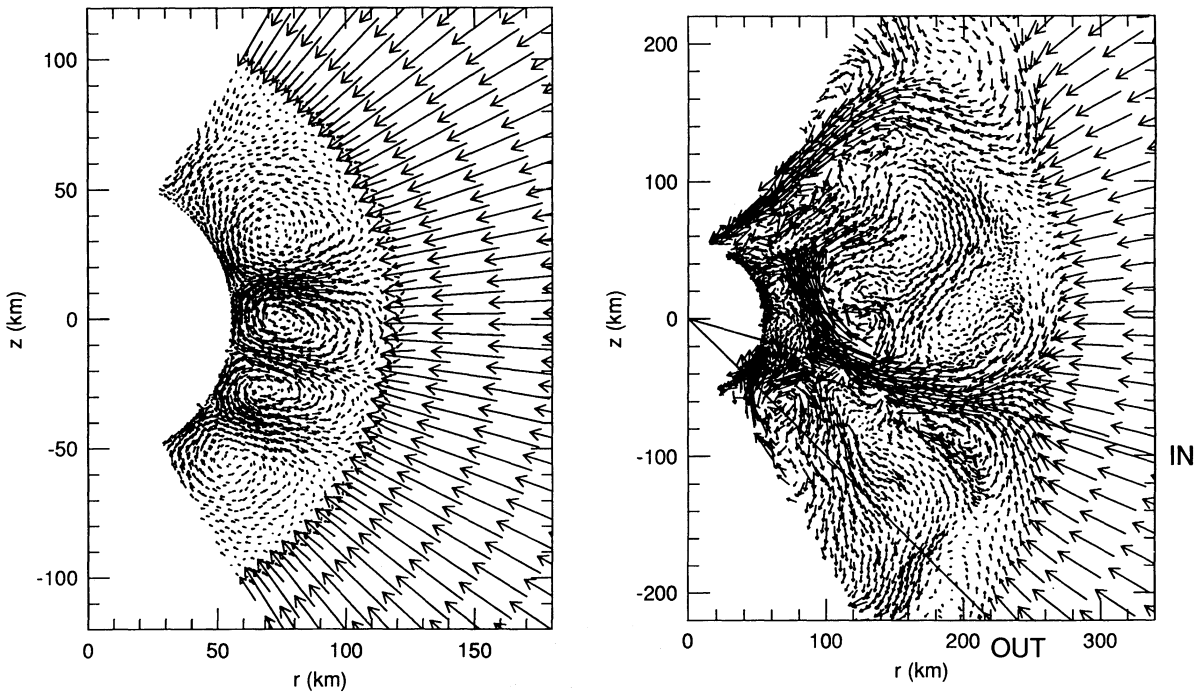

FIG. 5.—Velocity plots for model B at $t = 14$ ms (*left*), and $t = 38$ ms (*right*). Velocities are scaled independently for each plot.

the shock which collects the still low entropy matter which has just been overtaken by the shock and sends it toward the proto–neutron star. As this infalling stream moves down to smaller radii, it is choked, and hence weakly shocked again. When it reaches the immediate vicinity of the proto–neutron star, it is further heated by neutrino energy deposition. The previously down-flowing material then becomes buoyant and feeds the high-entropy bubble of rising matter. The inflow and outflow remain coherent over long distances and therefore do not lead to intimate mixing nor do they homogenize the entropy distribution behind the shock. The accreted mass is small: a few $10^{-2}\ M_{\odot}$, but as we point out in § 2.5, this is an aspect of the physics which we do not claim to model very well for the moment. At still later times ($t > 500$ ms), the rarefaction wave as well as the high-entropy bubble are left far behind by the shock as it runs down the density gradient of the stellar envelope (Fig. 9).

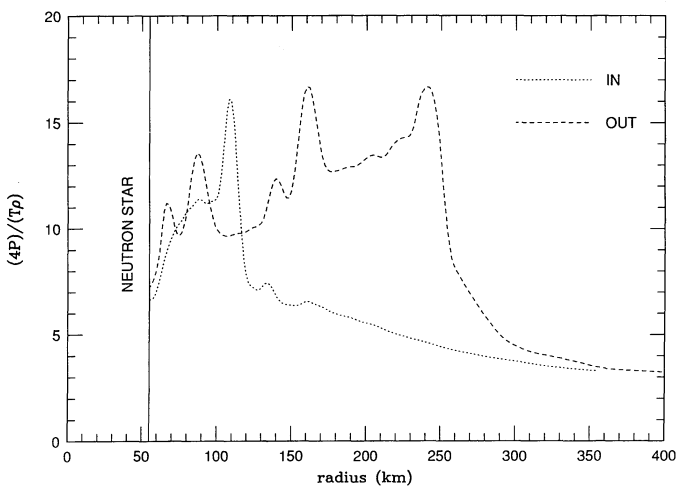

FIG. 6.—Plot of the quantity $4P/(T\rho)$ in k_B/nucleon (approximately the entropy), corresponding to the lines "in" and "out" of Fig. 5 (*right*). Note that the shock is nearly undetectable because most of the entropy jump is taken up by the dissociation of heavy nuclei.

It is remarkable that in each of our simulations of model B, the final flow pattern soon developed the largest eddy size possible within the computational domain. We do not seed the instabilities with any perturbations and the initial conditions are perfectly spherically symmetric. Moreover, we have tried to eliminate all systematic numerical effects which might seed the instability, so that the instabilities grow from purely numerical noise. Notice that due to the discreteness of the SPH method, this numerical noise is larger than the one obtained with finite-difference methods. We expect that random fluctuations at a level of 10^{-3} are present in the determination of the hydrodynamical quantities, well above the usual 10^{-5} due to limited machine precision. Experiments run with 60°, 90°, and 120° wedges all give similar convective flows.

Despite the fact that the initial condition is spherically symmetric and the fact that the boundaries are periodic, the two-dimensional geometry and size of the computational space naturally introduces a scale size to the problem. In order to investigate the robustness of this tendency to select the lowest possible mode we have run an experiment with strong seed perturbations of a higher mode. To this end, the density of the infalling envelope was altered by a coherent sinusoidal perturbation with polar angle (sin 12θ) of amplitude $\pm 10\%$. It can be seen (Fig. 8) that eight convective cells appear very early on, but gradually merge together to form a pattern similar to the one obtained in the unperturbed case. This plainly shows that the preferred mode is the lowest one afforded by the computational domain. Clearly, this analysis may not apply to the real, three-dimensional, situation. However, it strongly suggests the possibility of a low order ($l = 1$ or $l = 2$) mode in three

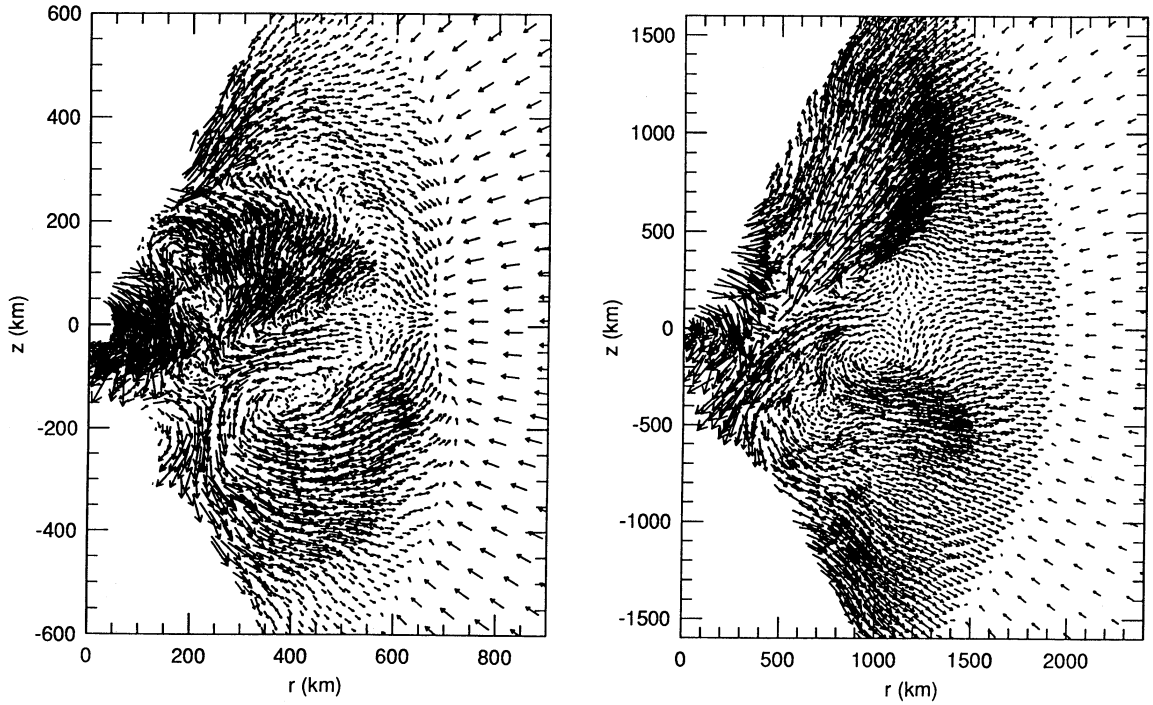

FIG. 7.—Velocity plots for model B at $t = 104$ ms (*left*), and $t = 228$ ms (*right*). Velocities are scaled independently for each plot.

dimensions, possibly seeded by rotation. We are currently investigating three-dimensional behavior, but since it is a computational task at least one order of magnitude beyond the two-dimensional case, it may remain beyond our capabilities for the moment.

As a direct result of the large-scale convective flows, the spatial distribution of ^{56}Ni of model B strongly departs from spherical symmetry. Figure 9 shows that at $t = 2.8$ s, after the post-shock temperature has decreased below 5×10^9 K and most of the material within the radius of the shock has recombined to ^{56}Ni, the nickel is concentrated in a rising bubble of high-entropy matter which follows behind the shock while unprocessed matter (mainly ^{16}O) caught up in the rarefaction wave sinks toward the neutron star. At $t = 2.8$ s, ^{56}Ni (0.05 $M_\odot$) has been mixed out to 0.15 $M_\odot$ beyond the mass cut (model B). In addition to this chemical inhomogeneity of the

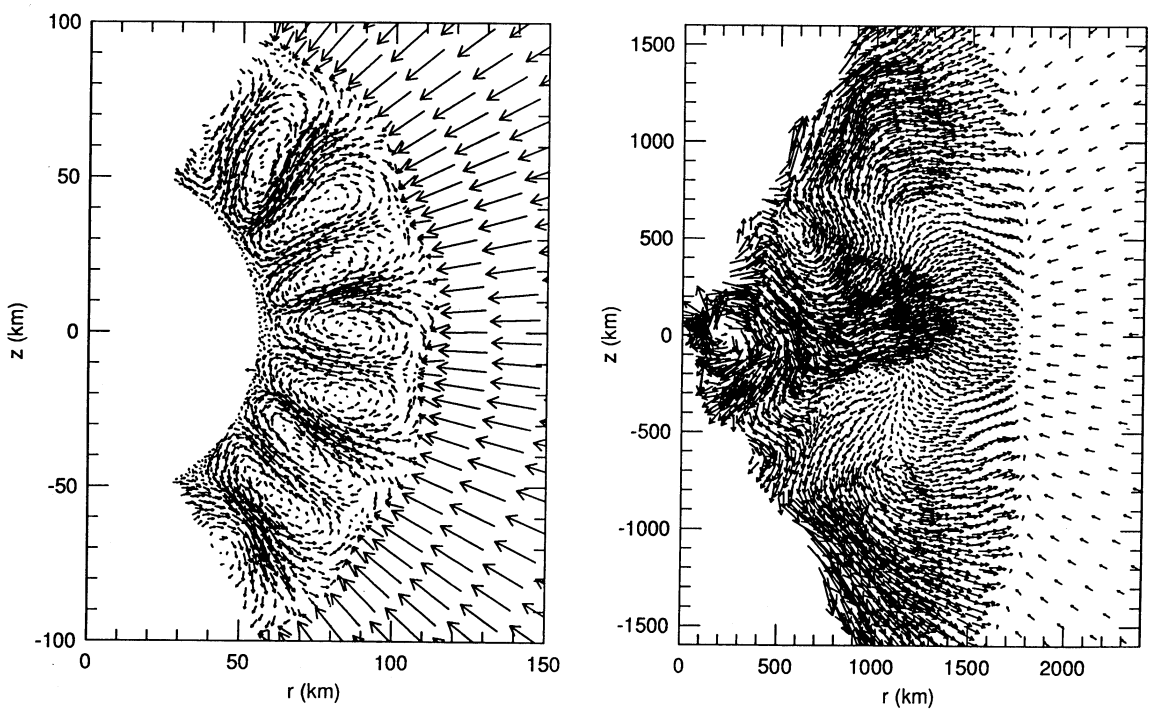

FIG. 8.—Velocity plots for model B with a strong initial sinusoidal density perturbations of wavelength 30°. Times are $t = 11$ ms (*left*) and $t = 220$ ms (*right*). Velocities are scaled independently for each plot.

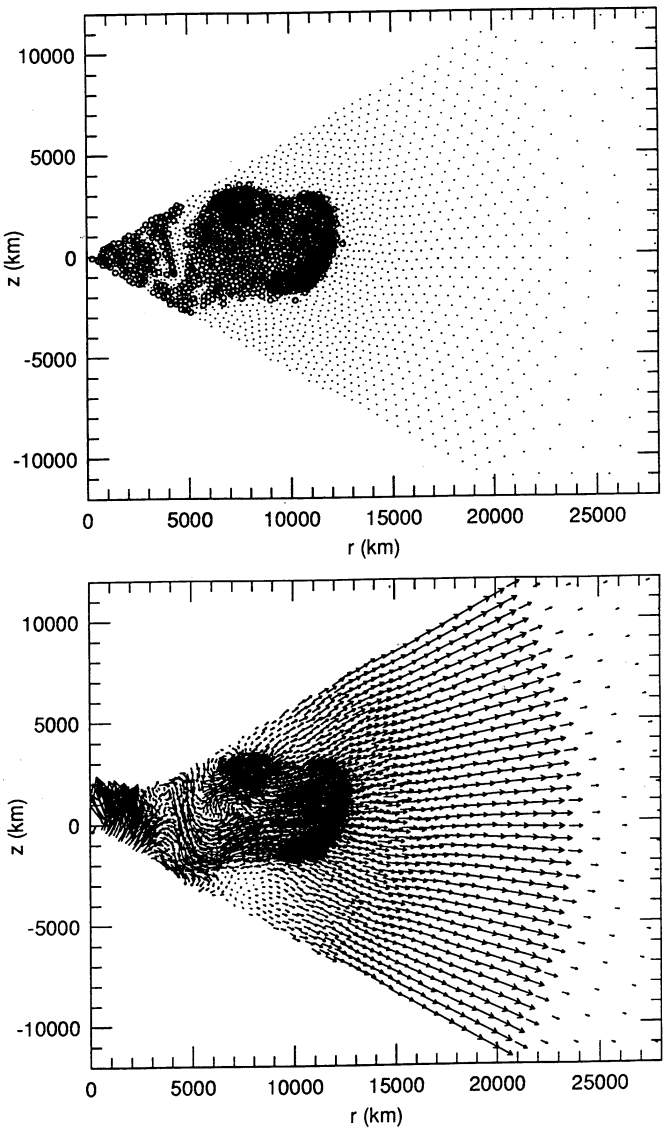

FIG. 9.—Velocity plot and particle plot at $t = 2.8$ s with nickel particles as thick dots.

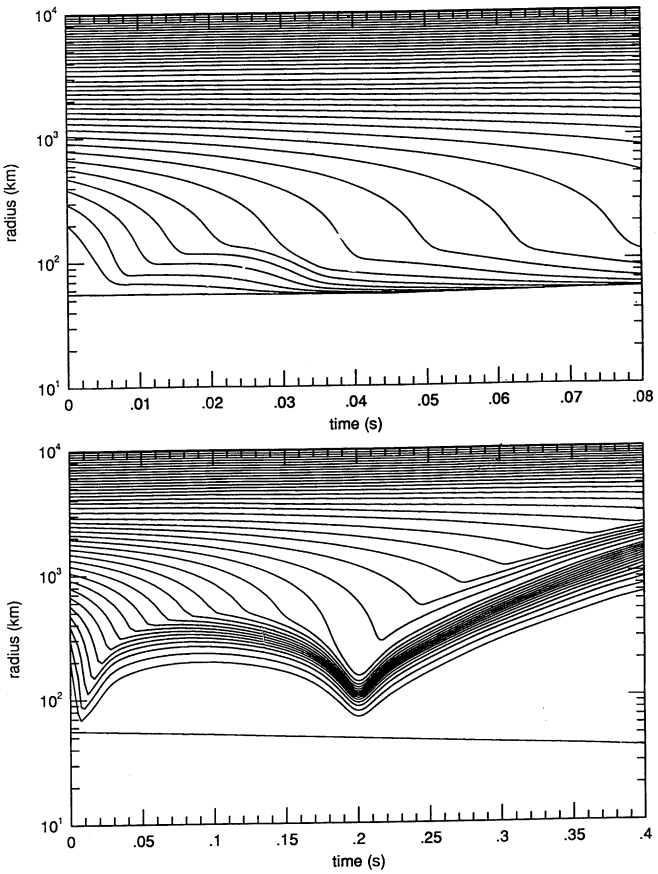

FIG. 10.—Worldline plots from one-dimensional simulations of model B with and without neutrino cooling.

expanding material behind the shock, the shock itself is nonspherical, assuming the shape of an oblate spheroid. This is especially evident in our 120° wedge simulations of model B where the initial major to minor axis radius ratio starts out as large as 1.4 and is still of order 1.2 at $t = 0.4$ s. It is not clear if this asymmetry will persist as the shock propagates through the rest of the star.

To investigate the effects of convection, we have performed a number of numerical experiments with a one-dimensional code. The starting condition was model B of the SPH simulations. Figure 10 (*top*) shows a plot of the worldlines of a sample of mass elements for a simulation which includes the exact same physics (except convection) as the SPH calculations. After an initial expansion of the inner zones during the first 20 ms, the explosion clearly fizzles, and matter accretes at a high rate onto the proto–neutron star. Suspecting that the origin of the failure was to be found in neutrino cooling losses, we ran the same simulation with all neutrino cooling turned off (Fig. 10, *bottom*). During the first 0.2 s, an atmosphere is formed around the proto–neutron star which goes through an oscillatory bounce. After this initial period, the shock takes off in a full-fledged explosion. This time delay in getting the explosion going should not be attributed to a delay in the energy deposition from neutrinos since most of the deposition takes place during the first 100 ms. Instead, the delay is due to the downward momentum flux from the infall which stalls the shock until the infalling matter thins out sufficiently to let it move out. Although these experiments certainly do not match the degree of sophistication of one-dimensional investigations by Wilson and Mayle, Bruenn, etc., we feel they clearly underline the importance of the large-scale, entropy preserving flows which we observe in our multidimensional simulations. We note here that Wilson and Mayle do not get explosions either if they turn off their convection algorithm in their one-dimensional code.

4. DISCUSSION

It is interesting that even though model A and B differ only by the duration of the infall until bounce and neutrino heating (respectively, 0.4 and 0.7 s), they produce radically different outcomes. Since model A corresponds to an earlier time in the collapse, the mass rate of infall is larger. As a result, densities are higher ahead and behind the shock, and there is a further increase of the density in the post-shock region by the compression due to the momentum flux carried by the infall. The post-shock material becomes degenerate and cooling losses

(see § 2.4) cripple the explosion. Because model B corresponds to a later time when the infall has significantly diminished, the runaway cooling induced by degeneracy is avoided, and convection is able to begin. We have also performed simulations of intermediate initial conditions between models A and B. We have found that a time delay of 0.5 s until bounce (proto–neutron star baryon mass of 1.44 $M_\odot$) fizzles while the 0.6 s (1.47 $M_\odot$) case explodes successfully. It thus appears that in order to prime the convective process and allow a successful explosion to develop, suitable initial conditions which preempt the onset of degeneracy by maintaining a low enough density or a high enough entropy are needed. In that respect, it is likely that our neglect of some of the bounce shock energy has important consequences for the subsequent evolution; in the real situation, the bounce shock increases the entropy by a significant factor out to a radius of order 200 km (S. W. Bruenn, private communication) and should prevent degeneracy from setting in. This makes us optimistic that once realistic initial conditions are used, explosions will be obtained more consistently.

The comparison between one-dimensional and two-dimensional simulation shows without ambiguity that convection plays a crucial role in ensuring an efficient explosion for model B. Bethe (1990) already pointed out that convection, by preventing material from reaching too high a temperature, can limit the neutrino cooling losses which were shown in § 2.4 to be proportional to T^6 or T^9, in the cases where electron-position pairs are important. In the absence of convection, the heating process is quickly balanced by the neutrino cooling; any increase in heating then results in more cooling. In simulation B, heated material is constantly expelled by buoyancy from the vicinity of the proto–neutron star and replaced by colder material. Further, during the early phase of the explosion, two additional factors combine to make the large-scale convective flow a formidably efficient way to transport energy. The first is that in effect, the material surrounding the proto-neutron star forms a binary mixture, one phase consisting of alpha particles, the other being free nucleons. As matter falls inward in a downflow, it is cold and mostly in the form of alpha particles. As the matter is heated, it is dissociated into free nucleons and finally ends up expelled in an outflow, where is eventually recombines and therefore restitutes the dissociation energy. This latent heat enables the storage of very large amount of energy without unduly raising the temperature, thus turning the heart of a supernova explosion into the ultimate steam engine.

The second point is that, very quickly, the scale height of the convective flow becomes comparable to the distance to the center and therefore, the up and down flows become individually entropy preserving. This allows a large geometrical expansion factor for a parcel of gas starting from the bottom of the flow and moving to the top of the cell. Note that this happens because a near constant entropy atmosphere is scale invariant and that a given parcel retains its shape independently of the radius to which it is transported. As a result, the efficiency of convective transport of energy to the shock is yet once again enhanced.

Chandrasekhar (1961) has shown that at the onset of convection in a spherical shell, the larger the ratio of the radius of the outer boundary to the radius of the inner boundary, the lower the order of the first growing mode. In the limit of a pointlike heat source, the $l = 1$ mode dominates. Obviously, the linear stability analysis of Chandrasekhar (1961) is not directly applicable here, since the behavior of the convective atmosphere around the proto–neutron star clearly corresponds to a highly nonlinear situation. However, numerical experiments (J. Baumgardner, private communication) have shown that even in regimes which are very far from the onset of the thermal instability, the dominant mode is still the one predicted by a stability analysis. As the shock quickly moves outward, the radius of the shock becomes much greater than the radius of the proto–neutron star, and one therefore expects a low-order mode of convection. While we reiterate that our two-dimensional simulations need to be complemented with a calculation in three dimensions in order to determine which is the preferred mode, the possibility that the $l = 1$ mode might be dominant would have interesting consequences. In a comprehensive study of neutron star birth and evolution, Dewey & Cordes (1987) claim that the observed velocity dispersion of pulsars cannot simply be explained by the disruptive effect of a supernova explosion in a binary system (see also Frail & Kulkarni 1991, on the discovery of a pulsar with a kick velocity possibly as high as 2000 km s^{-1}). They argue that it is necessary to invoke a kick velocity of order 100 km s^{-1} imparted to the pulsar at birth, which presumably would be related to the explosion mechanism itself. The asymmetry of a $l = 1$ convective mode leading to preferential accretion on one side of the proto–neutron star might offer an explanation for such kick velocities (the idea of a convective overturn imparting a kick velocity was already mentioned by Arnett 1987). Because typical velocities of the flows in the bubble are of order $c/10$, an asymmetry involving a mass of order 10^{-2} $M_\odot$ is all that is needed to give $\Delta v \sim 100$ km s^{-1} for the neutron star. Finally, if the $l = 1$ mode did indeed dominate in SN 1987A, it may provide an answer to the systematic redshifts observed by Tueller et al. (1990), Haas et al. (1990), and Spyromilio et al. (1990) in cobalt and iron lines, assuming that the direction of the main outflow was directed away from us.

For model B, the explosion energy ($\sim$0.35 foe) is definitely on the low side compared to the $\sim$1.4 foe inferred from observations of SN 1987A. However, we would like to point out that we have been systematically conservative in our assumptions for the energy input. It is probable that an increased neutrino flux and/or temperature generated by accretion of matter onto the proto–neutron star (which would still have to satisfy the constraints imposed by the neutrino detections on Earth) or additional neutrino processes which we do not take into account (such as $\nu\bar{\nu}$ annihilation in electron-positron pairs or neutrino-nucleus interactions) could raise the explosion energy toward a more acceptable value. Our neglect of the energy contribution of the prompt shock may be blamed for our low explosion energies. On the other hand, the fact that model B produces an amount ^{56}Ni fairly close to the required amount (0.05 $M_\odot$ vs. 0.075 $M_\odot$) seems to rule out a large increase in the energy deposition without a concomitant increase in the accretion. We believe that this points directly toward accretion as an additional source of energy powering the explosion after the first 100 ms, while removing the "excess" nickel. Within this picture, the persistence of downward, low-entropy flows fuels the accretion and provides an additional source of neutrinos with which to heat material (see § 2.5). This mechanism is *self-regulating* in the sense that the energy input will be turned off only by the cessation of the downward flows which itself is conditional to the success of the explosion (Colgate et al. 1992). As H. Bethe has put it, convection allows accretion, and therefore neutrino heating, to continue, even when the shock is moving outward in radius, thereby maintaining an energy input to the explosion and guaranteeing its success.

Our results show that for a successful explosion, the post-shock structure is strongly spatially inhomogeneous. This will certainly have a substantial impact on the subsequent RT instabilities which are thought to occur at the He/H and CO/He interfaces. So far, all simulations of these RT instabilities (such as in Hachis et al. 1990; Fryxell, Arnett, & Müller 1991; HB91 and HB92) have relied on an initial conditions obtained by a one-dimensional evolution of the explosion which implicitly assumes a high degree of spherical symmetry. To what extent the new picture will modify these results remains to be seen. However, one can already point out that the large-scale inhomogeneity of the nickel distribution will have a significant effect on the late-time ($t >$ few days) optical display of the supernova as it begins to be powered by the radioactive decays of ^{56}Ni and ^{56}Co. Furthermore, Chevalier & Soker (1989), and Yamada & Sato (1990) have shown that an initial explosion asymmetry can persist after the propagation of the shock through the stellar envelope and lead to an asymmetric expansion of the ejecta. These two factors may be the explanation for the multiple indications of asymmetry in SN 1987A pointed out by Jeffery (1991), Phillips & Heathcote (1989), and Papaliolios et al. (1989). Finally, HB92 have argued that the high-velocity tail of the iron distribution observed by Hass et al. (1990), and Spyromilio et al. (1990) could be explained by the RT instabilities provided some nickel was premixed to 1.5 $M_\odot$ above the mass cut. The amount of premixing we obtain is smaller than that, but is still increasing by the end of our simulations. Considering that the RT instabilities do not show significant growth until at least 15 minutes after the explosion, it is not unreasonable to think that a sufficient level of premixing may be attained within that time span, and thus resolve the nickel discrepancy. As the explosion progresses, convection slows and eventually stops as the radius reached by the high-entropy bubble increases and thus, gravity which drives buoyancy decreases. Figure 9 is indicative of this, since it shows that at $t = 2.8$ s, the bubble is far behind the shock which moves at an almost constant velocity.

The authors are aware that the results which are presented in this paper are incomplete and possibly raise as many questions as they try to answer. First and foremost, the initial conditions have to be refined to a more realistic collapse solution, with self-consistent neutrino emission from the proto–neutron star. Another important issue to be resolved is the physical behavior of an accreting atmosphere onto a proto–neutron star. As mentioned above, this may be the key to a robust explosion mechanism. This problem is addressed in Colgate et al. (1992) and will continue to be investigated on our part with the ultimate objective of developing an accretion algorithm applicable to multidimensional simulations. The three-dimensional case needs to be investigated as well as the late-time behavior of the explosion. The physics of the neutrino energy deposition should be improved to take into account all the processes we have so far left out under the assumption that they are not important. To achieve this, it will be necessary to dynamically evolve the local Y_e during the simulation. Finally, the implications of the multidimensional character of the explosion for nucleosynthesis need to be explored in detail. In that respect, chemical abundances constraints, including those related to the *r*-process element, should provide useful diagnostics with which to rule out or support alternative models. Despite all these caveats, there are now strong indications that multidimensional hydrodynamics play a fundamental role in SN II explosions. If this is the case, it will clearly affect our entire understanding of the behavior of SN IIs.

We would like to thank J. Baumgardner, S. Bruenn, A. Burrows, M. B. Davies, B. Fryxell, R. Hix, P. Pinto, F.-K Thielemann, and S. Woosley for suggestions and enlightening discussions. We are also indebted to the referee (J. Wilson) for pointing out several mistakes in the original version of this paper. Calculations of NSE abundances versus temperature and density were performed by R. Hix. The progenitor model of SN 1987A was supplied to us by K. Nomoto. S. A. C. acknowledges the support of the Department of Energy. W. B. and M. H. acknowledge the support of NASA grant NGR 22-007-272 at Harvard University and NSF grant AST 9206378 at the University of Arizona as well as the support of the Theory Division at the Los Alamos National Laboratory during their visits there.

REFERENCES

Anzer, U., Borner, G., & Monaghan, J. J. 1987, A&A, 176, 235
Arnett, W. D. 1977, ApJ, 218, 815
———. 1987, in IAU Symp. 125, The Origin and Evolution of Neutron Stars, ed. D. J. Helfand & J.-H. Huang (Dordrecht: Reidel), 273
Arnett, W. D., Bahcall, J. N., Kirshner, R. P., & Woosley, S. E. 1989, ARA&A, 27, 629
Baron, E. A., & Cooperstein, J. 1990, ApJ, 353, 597
Benz, W. 1991, in Late Stages of Stellar Evolution and Computational Methods in Astrophysical Hydrodynamics, ed. C. de Loore (Berlin: Springer), 259
Bethe, H. A. 1990, Rev. Mod. Phys., 62, 801
Bludman, S. A., & Schinder, P. J. 1988, ApJ, 326, 265
Braaten, E. 1991, Phys. Rev. Lett., 66, 13
Bruenn, S. W. 1985, ApJS, 58, 771
Bruenn, S. W., & Haxton, W. C. 1991, ApJ, 376, 678
Burrows, A. 1988, ApJ, 334, 891
Chandrasekhar, S. 1961, Hydrodynamic and Hydromagnetic Stability (New York: Dover)
Chevalier, R. A., & Soker, N. 1989, ApJ, 341, 867
Colgate, S. A., Herant, M., & Benz, W. 1992, Phys. Rep., in preparation
Colgate, S. A., & Johnson, M. H. 1960, Phys. Rev. Lett., 5, 235
Colgate, S. A., & White, R. H. 1965, ApJ, 143, 626
Dewey, R. J., & Cordes, J. M. 1987, ApJ, 312, 780
Fryxell, B., Arnett, W. D., & Müller, E. 1991, ApJ, 367, 619
Frail, D. A., & Kulkarni, S. R. 1991, Nature, 352, 785
Goodman, J., Dar, A., & Nussinov, S. 1987, ApJ, 314, L7
Hachisu, I., Matsuda, T., Nomoto, K., & Shigeyama, T. 1990, ApJ, 358, L57
Haas, M. R., Colgan, S. W. J., Erickson, E. F., Lord, S. D., Burton, M. G., & Hollenbach, D. J. 1990, ApJ, 360, 257
Herant, M. 1992, Ph.D. thesis, Harvard University
Herant, M., Benz, W. 1991, ApJ, 370, L81 (HB91)
———. 1992, ApJ, 387, 294 (HB92)
Janka, H.-Th. 1991, A&A, 244, 378
Jeffery, D. J. 1991, ApJ, 375, 264
Matz, S. M., Share, G. H., Leising, M. D., Chupp, E. L., Vestrand, W. T., Purcell, W. R., Strickman, M. S., & Reppin, C. 1988, Nature, 331, 416
Mayle, R. W., & Wilson, J. R. 1991, in Supernovae, ed. S. E. Woosley (New York: Springer), 33
Papaliolios, C., Karovska, M., Koechlin, L., Nisenson, P., Standley, C., & Heathcote, S. 1989, Nature, 338, 565
Phillips, M. M., & Heathcote, S. R. 1989, PASP, 101, 137
Schinder, P. J., Schramm, D. N., Wiita, P. J., Margolis, S. H., & Tubbs, D. L. 1987, ApJ, 313, 531
Shigeyama, T., & Nomoto, K. 1990, ApJ, 360, 242
Shigeyama, T., Nomoto, K., & Hashimoto, M. 1988, A&A, 196, 141
Spyromilio, J., Meikle, W. P. S., & Allen, D. A. 1990, MNRAS, 242, 669
Takahashi, K., El Eid, M. F., & Hillebrandt, W. 1978, A&A, 67, 185
Tueller, J., Barthelemy, S., Gehrels, N., Teegarden, B. J., Leventhal, M., & MacCallum, C. J. 1990, ApJ, 351, L41
Wilson, J. R. 1985, in Numerical Astrophysics, ed. J. M. Centrela, J. M. LeBlanc, & R. L. Bowers (Boston: Jones & Barlett), 422
Wilson, J. R., & Mayle, R. W. 1989, presented at Supernovae and Stellar Collapse, Conference on Nuclear Equation of State, Peniscola, Spain, unpublished
Woosley, S. E., & Weaver, T. A. 1986, ARA&A, 24, 205
Yahil, A. 1983, ApJ, 265, 1047
Yamada, S., & Sato, K. 1990, ApJ, 358, L9